Extraordinary Permittivity Characterization Using 4H-SiC Substrate-Integrated-Waveguide Resonators

Lei Li[1], Steve Reyes[2], Mohammad Javad Asadi[1], Xiaopeng Wang[1], Gianluca Fabi[1], Erdem Ozdemir[1], Weifeng Wu[3], Patrick Fay[3], James C. M. Hwang[1]
[1]Cornell University, Ithaca, NY, USA, [2]Anritsu Company, Morgan Hill, CA, USA
[3]University of Notre Dame, South Bend, IN, USA

2023 100th ARFTG Microwave Measurement Conference (ARFTG) | 978-1-6654-7494-8/23/$31.00 ©2023 IEEE | DOI: 10.1109/ARFTG56062.2023.10148877

***Abstract* — Currently, lacking suitable test structures, little data exist for the permittivity of hexagonal materials such as GaN and SiC at millimeter-wave frequencies, especially for the extraordinary permittivity $\varepsilon_{\|}$ as opposed to the ordinary permittivity $\varepsilon_{\perp}$. This paper demonstrates for the first time that it is possible to characterize $\varepsilon_{\|}$ of *c*-axis 4H SiC using on-wafer measurements of substrate-integrated-waveguide resonators. In fact, measurements on eleven resonators yield a relative $\varepsilon_{\|}$ of 10.27 ± 0.03 and a loss tangent tanδ < 0.02 over the D band (110–170 GHz). The on-wafer measurements of resonators and other devices fabricated on the same SiC substrate can allow material property to be closely correlated with device performance. The present approach can be extended to materials of other types and orientations.**

***Index Terms* — Calibration, complex permittivity, millimeter wave, on-wafer measurement, resonators, substrate-integrated waveguide.**

I. Introduction

Accurate modeling and characterization of material permittivity are critical for high-frequency devices above 110 GHz [1], [2]. However, little data exist at millimeter-wave frequencies and, when they exist, data characterized by different labs and techniques on the same material can differ by as much as 10% [3]. In particular, *c*-axis 4H-SiC is commonly used as the substrate for high-frequency, high-power GaN devices which are interconnected by microstrip or coplanar transmission lines. The TEM wave traveling on these transmission lines [Fig. 1(a) and Fig. 1(b)] is governed by both ordinary permittivity $\varepsilon_{\perp}$ and extraordinary permittivity $\varepsilon_{\|}$ perpendicular and parallel to the *c* axis, respectively [4]. For these applications, although there have been several reports of $\varepsilon_{\perp}$ for 4H SiC [5]–[10], there is no report of $\varepsilon_{\|}$ at millimeter-wave frequencies (Fig. 2). The only report of $\varepsilon_{\|}$ is at terahertz frequencies using optical means [9].

Contrary to conventional microstrip or coplanar transmission lines, the TE wave traveling in a substrate-integrated waveguide (SIW) fabricated on *c*-axis 4H-SiC is only governed by $\varepsilon_{\|}$ [Fig. 1(c)], greatly simplifying its modeling and characterization. Furthermore, we have shown [11] that, across the D band (110–170 GHz), such an SIW can have < 0.3 dB/mm insertion loss, which is several times less lossy than conventional microstrip or coplanar transmission lines. As the result, SIW resonators fabricated on the same SiC wafer have unloaded quality factor [12] $Q \approx 100$, allowing $\varepsilon_{\|}$ to be accurately extracted.

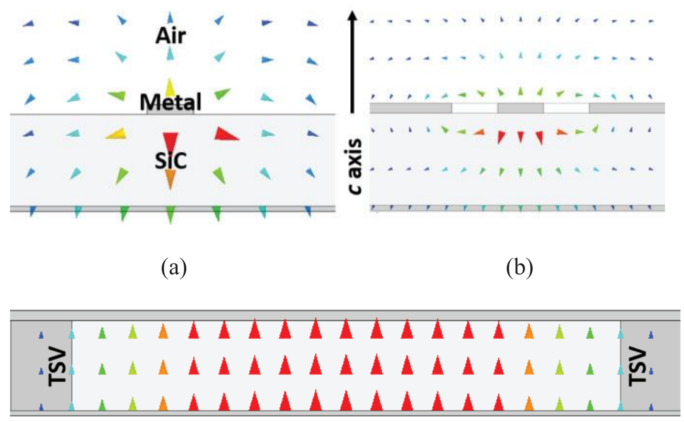

Fig. 1. Simulated cross-sectional distribution of electric field at 140 GHz for a 50-Ω (a) microstrip transmission line, (b) GCPW transmission line, and (c) SIW on a 50-μm-thick *c*-axis 4H-SiC substrate.

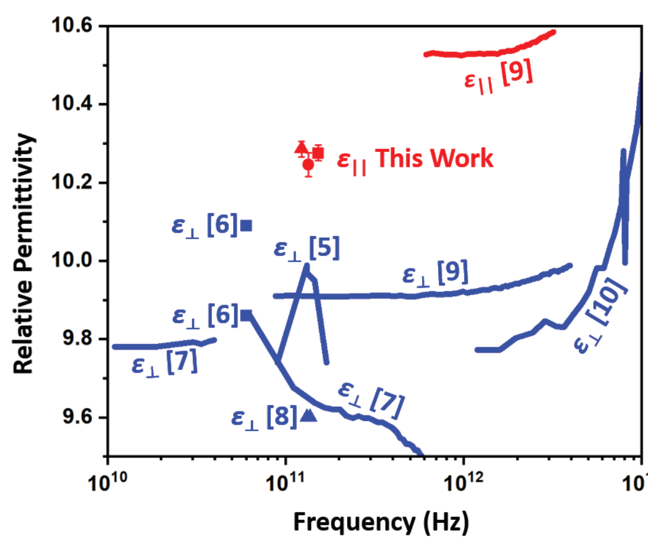

Fig. 2. Measured relative permittivity of 4H SiC [5]–[10]. This work reports average extraordinary permittivities and standard deviations extracted from three resonators at 123 GHz (▲), three resonators 134 GHz (●), and five resonators at 152 GHz (■), respectively.

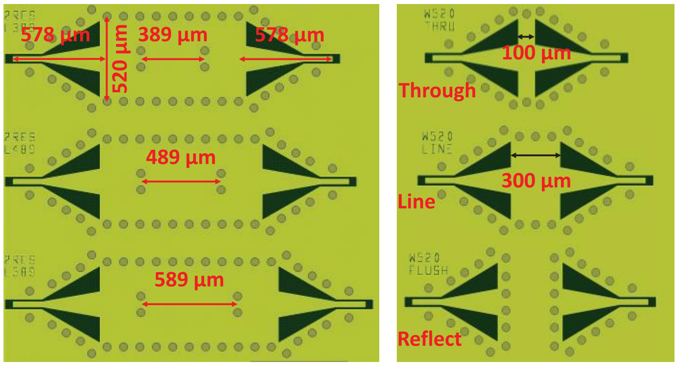

(a) (b)

Fig. 3. Composite (front and back) layout of (a) three SIW resonators with ℓ = 389, 489, and 589 µm, respectively, each resonator being sandwiched between two 578-µm-long SIW-GCPW transitions at the input and output, respectively, and (b) impedance standards "through," "line," and "reflect" fabricated on the same SiC wafer as the resonators.

II. Experiments

Fig. 3 illustrates the layouts of three types of SIW resonators with length ℓ = 389, 489, and 589 µm, respectively [11]. The resonators are fabricated together on 100-µm-thick *c*-axis 4H-SiC (Wolfspeed W4TRF0R-0200, > 10^5 Ω·cm resistivity). Each SIW is bound on the top and bottom with 0.1-µm-thick Ni and 0.7-µm-thick Al, and on the left and right with rows of through-substrate vias (TSVs). The TSVs are 45 µm in diameter and spaced 100 µm center-to-center. The length of each resonator is determined by irises each formed by a pair of TSVs optimally placed in the middle of the SIW. All resonators are 520-µm wide for the D-band operation. For on-wafer measurement, the input or output of each resonator is transitioned through a 578-µm-long tapered section to a grounded coplanar waveguide (GCPW). Each transition has < 0.2 dB insertion loss with minimum impact on measurement uncertainty [13]. For impedance standards, SIW-based "through," "line," and "reflect" are also laid out and fabricated on the same SiC wafer.

On-wafer measurement is based on 2-tier calibration, using both on-wafer and off-wafer impedance standards in conjunction with an Anritsu ME7838G 220-GHz vector network analyzer and two MPI TITAN 220-GHz coaxial probes with 50-µm pitch [13]. Tier-1 calibration is based the load-reflection-match method [14] using an MPI TCS-050-100-W impedance-standard substrate. Tier-2 calibration is based on the through-reflect-line method [15] using the impedance standards shown in Fig. 3(b). Tier-1 calibration establishes the reference plane at the probe tip 15 µm inside the end of the GCPW. Tier-2 calibration moves the reference plane past the GCPW-SIW transition by 50 µm to the middle of "through." After tier-2 calibration, the de-embedded scattering parameters of the intrinsic resonators are free from the effects of $\varepsilon_\perp$ and can be used to accurately extract $\varepsilon_\parallel$. In the future, with the GCPW-SIW transitions validated and repeatable, a single-tier calibration

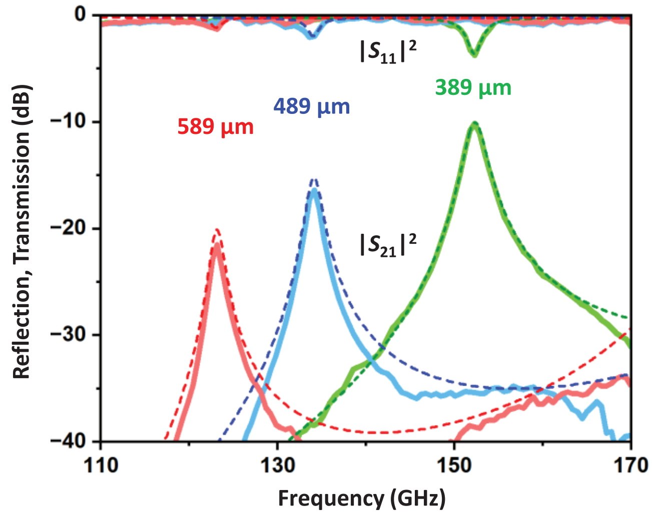

Fig. 4. Measured (solid) vs. simulated (dashed) $|S_{11}|$ and $|S_{21}|$ for intrinsic SIW resonators with ℓ = 389, 489, and 589 µm, respectively. The simulation is performed with $\varepsilon_\parallel$ = 10.27 and tanδ = 0.0001.

using the on-wafer impedance standards of Fig. 3(b) may be sufficient to extract the intrinsic SIW characteristics.

III. Results and Discussion

A. Relative Permittivity $\varepsilon_\parallel$

With the SIW-GCPW transitions de-embedded, Fig. 4 compares the measured and simulated magnitudes of the reflection and transmission coefficients ($|S_{11}|$ and $|S_{21}|$) of three intrinsic resonators. The simulation is performed by using the 3D finite-element full-wave simulator HFSS under the automatic adaptive meshing mode, with $\varepsilon_\parallel$ as a tuning parameter. It can be seen that resonances occur around 123, 134, and 153 GHz and Q = 89, 88, and 88 for ℓ = 589, 489, and 389 µm, respectively. Moreover, a relative $\varepsilon_\parallel$ = 10.27 and a loss tangent tanδ = 0.0001 [5], [8] can fit all three resonators. Statistically, eleven resonators are characterized. They indicate that $\varepsilon_\parallel$ = 10.29 ± 0.02 at 123.1 ± 0.1 GHz for three 589-µm-long resonators; $\varepsilon_\parallel$ = 10.25 ± 0.03 at 134.2 ± 0.3 GHz for three 489-µm-long resonators, and $\varepsilon_\parallel$ = 10.27 ± 0.02 at 152.3 ± 0.1 GHz for five 389-µm-long resonators. These results are included in Fig. 2. Since they exhibit little dispersion over the D band, the average over all eleven resonators yields $\varepsilon_\parallel$ = 10.27 ± 0.03, which differs significantly from that extrapolated from [9].

The above results confirm that $\varepsilon_\parallel$ can be extracted with better than 1% precision. The precision can be attributed to 1) homogenous medium (without air gap or surface contamination), 2) decoupling of $\varepsilon_\parallel$ from $\varepsilon_\perp$, and 3) resonance determined by lateral dimensions, which are controlled to within 0.1% by semiconductor processes.

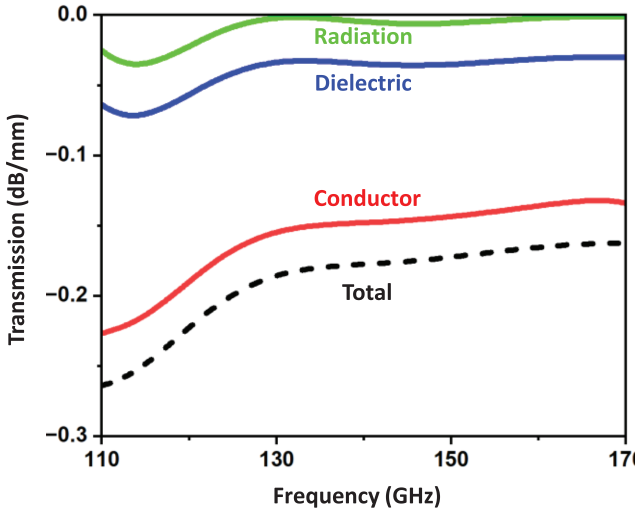

Fig. 5. Simulated SIW loss mechanisms with $\sigma = 4 \times 10^7$ S/m and tanδ = 0.001.

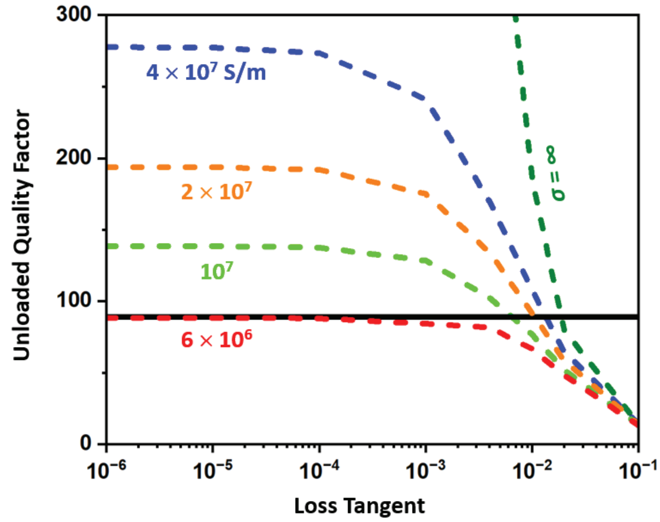

Fig. 6. Measured (solid) vs. simulated (dashed) Q as a function of tanδ with σ as a parameter for a 389-µm-long resonator.

B. Loss Tangent tanδ

The imaginary part of $\varepsilon_{\parallel}$ can be characterized by tanδ, which is critical to the resonator loss or Q. Presently, Q can only be used to determine the upper limit of tanδ because the resonator loss is dominated by the conductor loss instead of the dielectric loss. For example, Fig. 5 shows that the HFSS-simulated loss of the SIW with typical values of tanδ and the metal conductivity σ. It can be seen that the conductor loss dominates, consistent with other reports such as [16]. In turn, the conductor loss is dominated by σ instead of metal thickness or interface roughness because 1) at 0.8 µm, the conductor is much thicker than the skin depth at the D band, and 2) the present "epi ready" 4H SiC substrate has an average roughness of ± 3 nm, which is negligible compared to the wavelength at the D band. Thus, to precisely characterize the loss of 4H SiC, σ needs to be significantly improved.

Although presently there is no effective way to separate the effects of σ and tanδ on Q, it can be used to establish the lower limit of σ and the upper limit of tanδ. For a 389-µm-long resonator, Fig. 6 compares the measured Q = 89 (a horizonal solid line) with values simulated by different combinations of σ and tanδ (dashed curves). It can be deduced that $\sigma > 6 \times 10^6$ S/cm and tanδ < 0.02, because Q = 89 for $\sigma = 6 \times 10^6$ S/cm and tanδ = 0, as well as for $\sigma = \infty$ and tanδ = 0.02.

IV. Conclusion

Enabled by the SIW, the above results demonstrate consistent and precise on-wafer characterization of the extraordinary permittivity of 4H SiC over the D band. The resulted $\varepsilon_{\parallel}$ differs significantly from $\varepsilon_{\perp}$ reported for the D band and $\varepsilon_{\parallel}$ extrapolated from terahertz frequencies. In the future, better metallization can be used to quantify tanδ. Through on-wafer characterization of resonators and other devices fabricated on the same SiC substrate, material property can be closely correlated with device performance. By fabricating SIW resonators on off-axis 4H SiC (e.g., on a axis), $\varepsilon_{\perp}$ can be similarly extracted. The approach can be extended to characterize the permittivity of other materials such as high-resistivity Si, which is commonly used for monolithic microwave and millimeter-wave integrated circuits.

Acknowledgement

We appreciate the technical discussion with X. Shang. We thank the technical assistance by K. Nomoto, Y. Tang, and W. Zhao. This work is supported in part by the US National Science Foundation (NSF) under Grants ECCS-2117305, ECCS-2122323, and ECCS-2132329, the US Office of Naval Research under Grant N00014-21-1-2680, as well as the Semiconductor Research Corporation and the US Defense Advanced Research Projects Agency through the Joint University Microelectronics Program. This work is performed in part at the Cornell NanoScale Facility, an NNCI member supported by NSF Grant NNCI-2025233.

References

[1] U. Gustavsson *et al.,* "Implementation challenges and opportunities in beyond-5G and 6G communication," *IEEE J. Microw.,* vol. 1, no. 1, pp. 86–100, Jan. 2021.
[2] W. Hong *et al.,* "The role of millimeter-wave technologies in 5G/6G wireless communications," *IEEE J. Microw.,* vol. 1, no. 1, pp. 101–122, Jan. 2021.
[3] D. Allal *et al.,* "Comparison on material parameter measurements in the THz spectral range with optical, resonant and VNA-based set-ups," *EURAMET TC Proj. Final Rep.,* Jul. 2022. Available: https://www.euramet.org/technical-committees/tc-projects/details/project/comparison-on-material-parameter-measurements-in-the-thz-spectral-range-with-optical-resonant-and-v/.

[4] O. P. A. Lindquist *et al.,* “Ordinary and extraordinary dielectric functions of 4H– and 6H–SiC from 3.5 to 9.0 eV,” *J. Appl. Phys.,* vol. 78, no. 18, pp. 2715–2717, Apr. 2001.

[5] J. M. Dutta, G. Yu, and C. R. Jones, "Dielectric losses in SiC at millimeter wavelengths," *in Proc. Joint 31st Int. Conf. Infrared Millimeter Waves 14th Int. Conf. Terahertz Electro.,* Shanghai, China, Jun. 2006.

[6] S. Chen, M. N. Afsar, and D. Sakdatorn, "Dielectric-parameter measurements of SiC at millimeter and submillimeter wavelengths," *IEEE Trans. Instrum. Meas.,* vol. 57, no. 4, pp. 706–715, Apr. 2008.

[7] J. G. Hartnett, D. Mouneyrac, J. Krupka, J.-M. le Floch, M. E. Tobar, and D. Cros, “Microwave properties of semi-insulating silicon carbide between 10 and 40 GHz and at cryogenic temperatures,” *J. Appl. Phys.,* vol. 109, no. 6, p. 064107, Mar. 2011.

[8] C. R. Jones, J. Dutta, G. Yu, and Y. Gao, “Measurement of dielectric properties for low-loss materials at millimeter wavelengths,” *J. Infrared Millimeter Terahertz Waves,* vol. 32, no. 6, pp. 838–847, Jun. 2011.

[9] M. Naftaly, J. F. Molloy, B. Magnusson, Y. M. Andreev, and G. V. Lanskii, “Silicon carbide—A high-transparency nonlinear material for THz applications,” *Opt. Express,* vol. 24, no. 3, pp. 2590–2595, Feb. 2016.

[10] A. T. Tarekegne, B. Zhou, K. Kaltenecker, K. Iwaszczuk, S. Clark, and P. U. Jepsen, "Terahertz time-domain spectroscopy of zone-folded acoustic phonons in 4H and 6H silicon carbide," *Opt. Express,* vol. 27, no. 3, pp. 3618–3628, Jan. 2019.

[11] M. J. Asadi *et al,* “Substrate-integrated waveguides for monolithic integrated circuits above 110 GHz,” in *IEEE MTT-S Int. Microw. Symp. (IMS),* Atlanta, GA, USA, Jun. 2021, pp. 669−672.

[12] P. Krkotić, Q. Gallardo, N. D. Tagdulang, M. Pont, and J. M. O’Callaghan, "Algorithm for resonator parameter extraction from symmetrical and asymmetrical transmission responses," *IEEE Trans. Microw. Theory Techn.,* vol. 69, no. 8, pp. 3917−3926, Aug. 2021.

[13] L. Li *et al.,* "Single-sweep vs. banded characterizations of a D-band ultra-low-loss SiC substrate integrated waveguide," in *ARFTG Microw. Meas. Conf.,* Denver, CO, USA, Jun. 2022.

[14] A. Davidson, K. Jones, and E. Strid, "LRM and LRRM calibrations with automatic determination of load inductance," in *ARFTG Conf. Dig.,* Monterrey, CA, Nov. 1990, pp. 57–63.

[15] R. B. Marks, "A multiline method of network analyzer calibration," *IEEE Trans. Microw. Theory Techn.,* vol. 39, no. 7, pp. 1205–1215, Jul. 1991.

[16] S. Hu *et al.,* "THz-wave propagation characteristics of TSV-based transmission lines and interconnects," in *Proc. IEEE Electron. Compon. Technol. Conf.,* 2010, pp. 46–50.